Pramana – J. Phys. (2017) 89:14
DOI 10.1007/s12043-017-1406-z

Optical properties of boron-group (V) hexagonal nanowires: DFT investigation

B SANTHIBHUSHAN*, MAHESH SONI and ANURAG SRIVASTAVA

Advanced Materials Research Group, CNT Laboratory, ABV-Indian Institute of Information Technology and Management, Gwalior 474 010, India
*Corresponding author. E-mail: bsb8897@gmail.com

Published online 20 June 2017

Abstract. The paper presents structural, electronic and optical properties of boron-group V hexagonal nanowires (h-NW) within the framework of density functional theory. The h-NW of boron-group V compounds with an analogous diameter of 12 Å have been designed in (1 1 1) plane. Stability analysis performed through formation energies reveal that, the stability of these structures decreases with increasing atomic number of the group V element. The band nature predicts that these nanowires are good electrical conductors. Optical behaviour of the nanowires has been analysed through absorption coefficient, reflectivity, refractive index, optical conductivity and electron energy loss spectrum (EELS), that are computed from the frequency-dependent complex dielectric function. The analysis reveals high reactivity of BP and BAs h-NWs to the incident light especially in the IR and visible ranges, and the optical transparency of BN h-NW in the visible and UV ranges.

Keywords. Hexagonal nanowire; optical properties; stability; density functional theory.

PACS Nos 62.23.Hj; 31.15.E–; 78.67.Uh; 78.67.–n; 71.20.–b

1. Introduction

With declining natural fossil fuel sources and increasing global warming, the search for highly efficient clean renewable energy sources such as solar cells is in high demand. Studying the properties of III–V compound nanowires [1–4] for their application in photovoltaics, optoelectronics and nanoelectronic devices is on rise and has become an extensive area of research owing to their remarkable characteristics ranging from direct band gap to high drive currents. The direct band gap is an essential requirement for designing optoelectronic devices, while the high drive currents are essential for high power applications. A vast amount of research is currently being pursued on the III–V nanowire-based solar cells [5–8]. Though the III–V nanowire-based solar cells earlier observed to offer efficiencies of just 3–5%, a few years ago the researchers developed a solar cell based on InP nanowire that has a remarkable 13.8% efficiency [7].

An interesting character of the nanowires is that their structural, electronic, optical, mechanical and transport properties are highly dependent on their shape and size. This enabled the researchers to tune the properties of nanowires by giving them different shapes and sizes, which in turn makes them eligible for various applications. The hexagonal-shaped compound nanowires have already been experimentally grown by various researchers and characterized for possible applications in nanoelectronics and nanoscale photonics [9–11]. In this work, the hexagonal NWs of B-group V compounds (BN, BP, BAs, BSb) have been designed with an analogous diameter of 12 Å, to comparatively examine their properties at the same shape and size. Earlier, our group has studied the properties of BAs h-NW at different diameters viz. 5, 7 and 9 Å, and reported the proportionality between stability and size [12], where, hexagonal nanowire with higher diameter is witnessed to be the most stable. Keeping it in mind, we have considered sufficiently large diameter for h-NWs in the present work to obtain stable B-group V h-NWs.

2. Theoretical approach

The calculations have been performed using density functional theory (DFT)-based commercial *ab-initio* package Atomistix Toolkit-Virtual Nanolab (ATK-VNL) [13]. The h-NW structures of 12 Å diameter have been

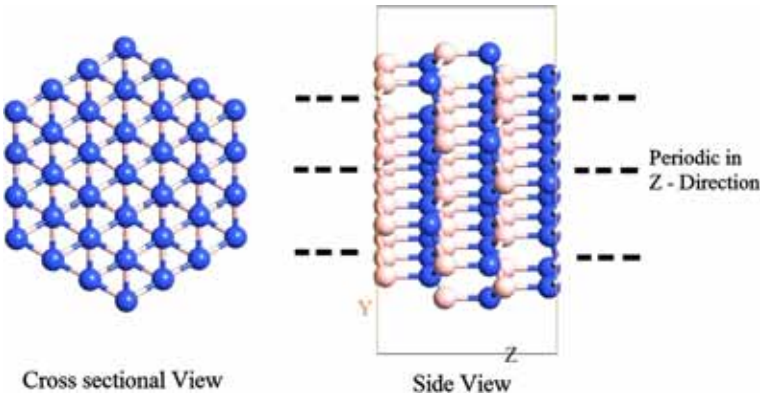

Figure 1. Cross-sectional view (across the length) and side view (along the length) of B-group V h-NW.

Table 1. Structural parameters and band nature for boron-group V h-NWs.

h-NW	B–V Bond length (Å)	Binding energy (eV)	Band gap (eV)
BN	1.56	8.14	SM
BP	1.96	6.06	M
BAs	2.06	5.38	SM
BSb	2.30 (W) 2.07 (L)	4.50	0.047

Here, M refers to metallic, SM to semimetallic, L to along length and W to along width.

designed by growing bulk structures of boron-group V compounds in (1 1 1) plane, and a model structure is depicted in figure 1. We utilized generalized gradient approximation (GGA) exchange-correlation functional with revised Perdew–Burke–Ernzerhoff (rPBE) parametrization [14] for calculating structural and electronic properties, and meta generalized gradient approximation (MGGA) [15] for calculating optical properties. MGGA is not preferred for the calculation of electronic properties, owing to its failure in accurately estimating the electronic properties of metallic structures. The valance electrons have been described using localized pseudoatomic orbitals with double zeta double polarized (DZDP) basis set, and a large plane-wave mesh-cutoff of 150 Ryd is considered throughout the calculations. Furthermore, the Brillouin zone (BZ) has been sampled using $1 \times 1 \times 40$ Monkhorst-Pack of k points.

3. Results and discussion

The hexagonal nanowires of boron-group V binary compounds with a diameter of 12 Å have been designed and their structural, electronic and optical properties have been calculated.

3.1 *Structural and electronic properties*

The structural parameters such as bond lengths and binding energies of B-group V h-NWs are calculated and presented in table 1, where one can observe the increasing pattern of the bond length with atomic number of group V element, reason being the dependence of bond length on size of the bonded atoms. In general, larger the size of the bonded atoms, larger will be the

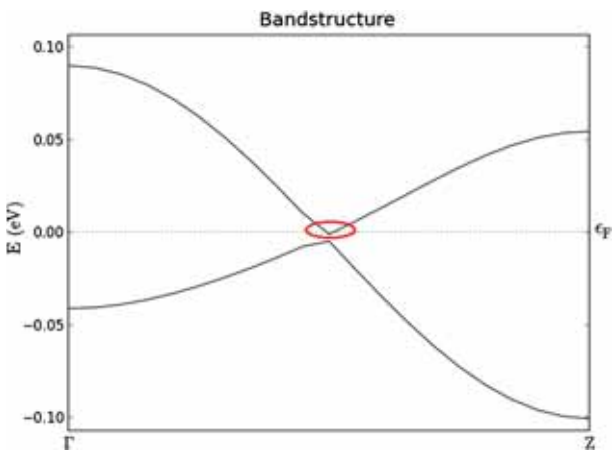

Figure 2. Band structure of BN h-NW.

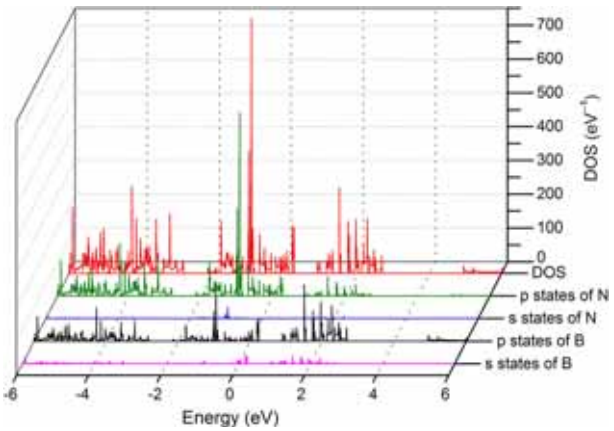

Figure 3. PDOS for BN h-NW.

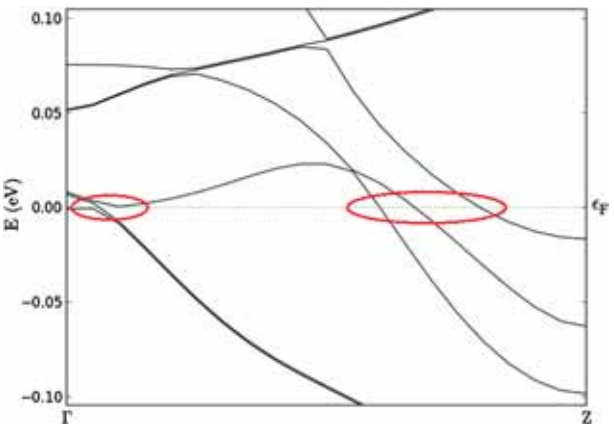

Figure 4. Band structure of BP h-NW.

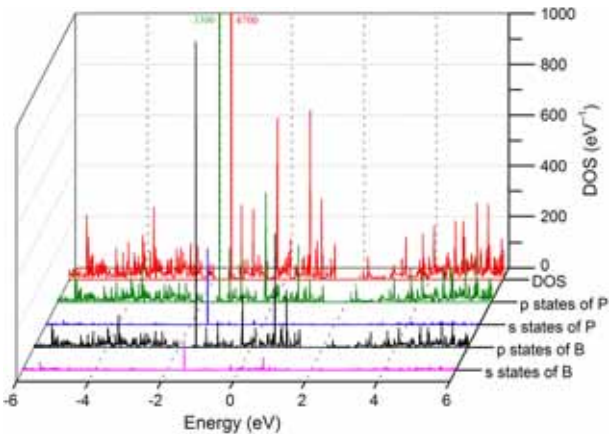

Figure 5. PDOS for BP h-NW.

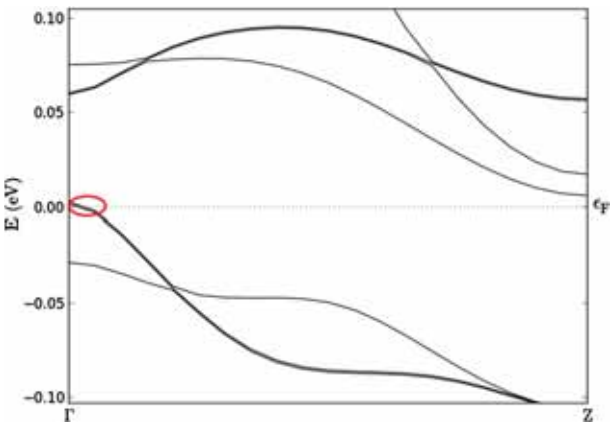

Figure 6. Band structure of BAs h-NW.

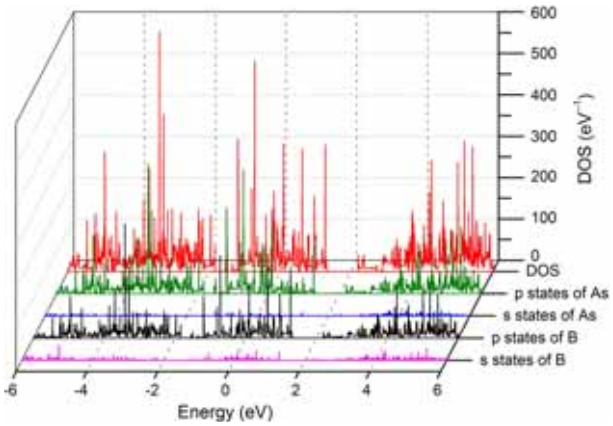

Figure 7. PDOS for BAs h-NW.

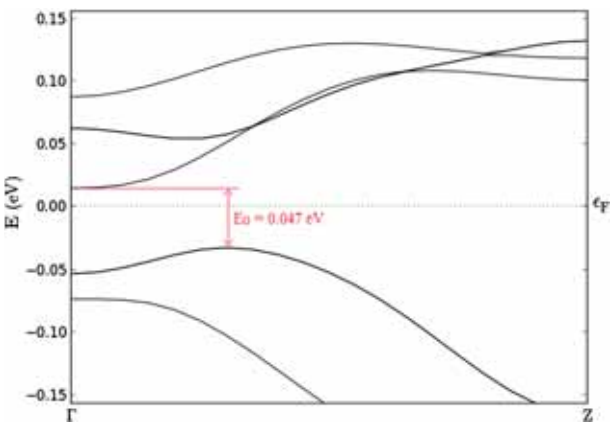

Figure 8. Band structure of BSb h-NW.

bond length, provided they have undergone analogous hybridization. Each of the h-NWs have shown unique bond length, which is same throughout their structure except for the case of BSb h-NW that shows different bond lengths along and across its length. The structural stability of h-NWs has been predicted through the calculated binding energies, where h-NW with the highest binding energy is presumed to be the most stable. The binding energies are calculated using the formula presented in eq. (1) and the corresponding values are listed in table 1. The binding energies are found to reduce with

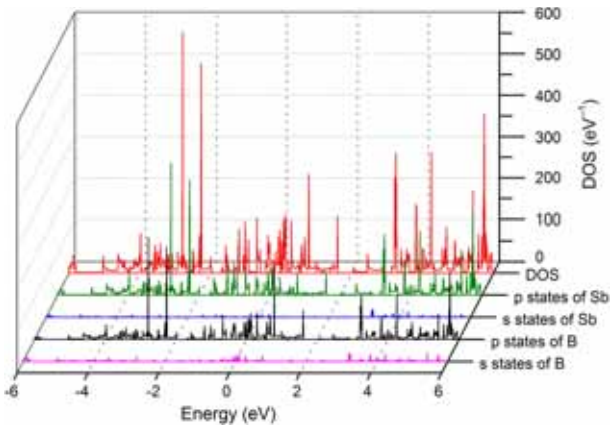

Figure 9. PDOS for BSb h-NW.

increasing atomic number of the group V element, predicting reduced stability with increasing atomic number of group V element. Here, BN h-NW is observed to be the most stable, whereas BSb h-NW is the least stable.

$$E_{\mathrm{B}} = \frac{N E_T(\text{boron}) + M E_T(\text{group V atom}) - E_T(\text{h-NW})}{(N+M)}. \tag{1}$$

The electronic nature of the B-group V h-NWs has been estimated through the band structure and projected density of states (PDOS) depicted in figures 2–9. BN and BAs h-NWs exhibit semimetallic nature, while BP h-NW exhibits metallicity. BSb h-NW shows a narrow band gap of 0.047 eV. Clearly, the band nature predicts good electrical conducting ability for the h-NWs. From PDOS plots, higher states density is observed in the valance band than in conduction band for all the four h-NW cases. Further, the states density observed in both valance and conduction bands is mainly due to the p states of boron and group V elements, reason being the involvement of p-orbitals in the formation of weak π-bonds which can be facilely disturbed to create free electrons, whereas, the contribution of s-states to DOS is near negligible in all the four h-NW cases as the s-orbitals are involved in the formation of strong σ-bonds.

3.2 *Optical properties*

The optical properties of B-group V h-NWs have been estimated through the absorption coefficient, reflectivity, refractive index, optical conductivity and electron energy loss spectra (EELS), that are calculated from the computed dielectric function over a photon energy range of 0–5 eV.

The frequency-dependent complex dielectric constant has been computed through the Kubo–Greenwood formulism for susceptibility tensor as shown in eq. (3), and the real and imaginary parts of the dielectric function are plotted in figures 10 and 11, respectively. The complex dielectric constant is related to the susceptibility tensor as [16]

$$\epsilon(\omega) = (1 + \chi_{ij}(\omega)), \tag{2}$$

$$\chi_{ij}(\omega) = \frac{-\mathrm{e}^2\hbar^4}{m^2\epsilon_0 V\omega^2}\Sigma_{nm} \times \frac{f(E_m) - f(E_n)}{E_{nm} - \hbar\omega - i\hbar\Gamma}\Pi^i_{nm}\Pi^j_{mn}, \tag{3}$$

where Π^i_{nm} is the i-component of the dipole matrix element between n and m states, V is the volume, $\hbar$ is the reduced Planck constant, Γ refers to broadening and f refers to Fermi function. The refractive index (n) and absorption coefficient (α) are calculated from the real part of the dielectric constant (ϵ_1) and imaginary part of the dielectric constant (ϵ_2) as

$$n = \sqrt{\frac{\sqrt{\epsilon_1^2 + \epsilon_2^2} + \epsilon_1}{2}} \tag{4}$$

$$\alpha = 2\frac{\omega}{c}k \tag{5}$$

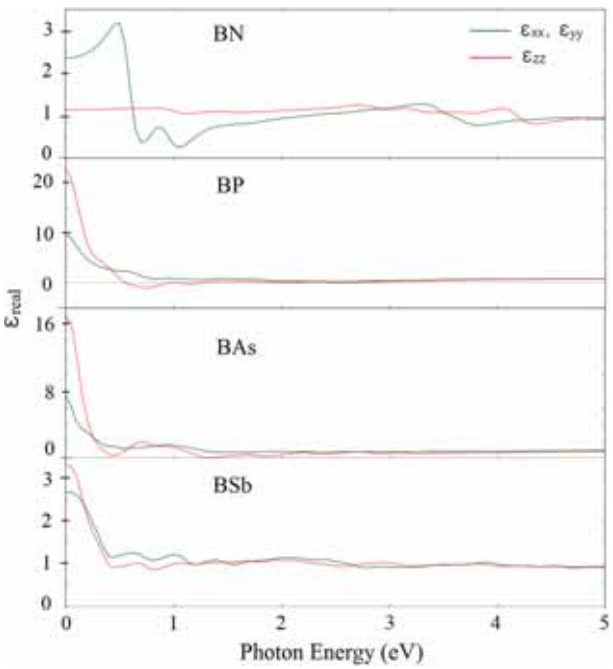

Figure 10. Real part of dielectric constant as a function of photon energy for B-group V h-NWs.

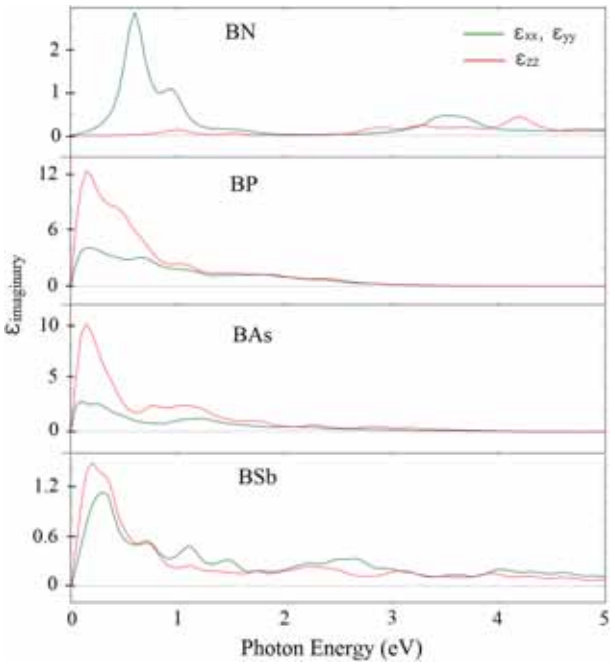

Figure 11. Imaginary part of dielectric constant as a function of photon energy for B-group V h-NWs.

where k is the extinction coefficient,

$$k = \sqrt{\frac{\sqrt{\epsilon_1^2 + \epsilon_2^2} - \epsilon_1}{2}}. \tag{6}$$

The optical reflectivity is calculated from the refractive index and extinction coefficient as

$$r = \frac{(1-n)^2 + k^2}{(1+n)^2 + k^2}. \tag{7}$$

The EELS is given by [17],

$$L = \frac{\epsilon_2}{\epsilon_1^2 + \epsilon_2^2}. \tag{8}$$

The real and imaginary parts of the optical conductivity, σ_{real} and $\sigma_{\text{imaginary}}$, are given by

$$\sigma_{\text{real}} = \frac{E\epsilon_2}{4\pi\hbar}. \tag{9}$$

$$\sigma_{\text{imaginary}} = \frac{E(1-\epsilon_1)}{4\pi\hbar}. \tag{10}$$

The dielectric function has been computed in three different directions ϵ_{xx}, ϵ_{yy} (across the NW length) and ϵ_{zz} (along the NW length). Owing to the periodic nature of the NW in Z-direction and confinement in X and Y directions, the dielectric function is observed to be anisotropic with $\epsilon_{xx} = \epsilon_{yy} \neq \epsilon_{zz}$. In figures 10–17, the calculated optical parameters across the length of the NW are indicated by dark green curve, while those along the length are indicated by red curve.

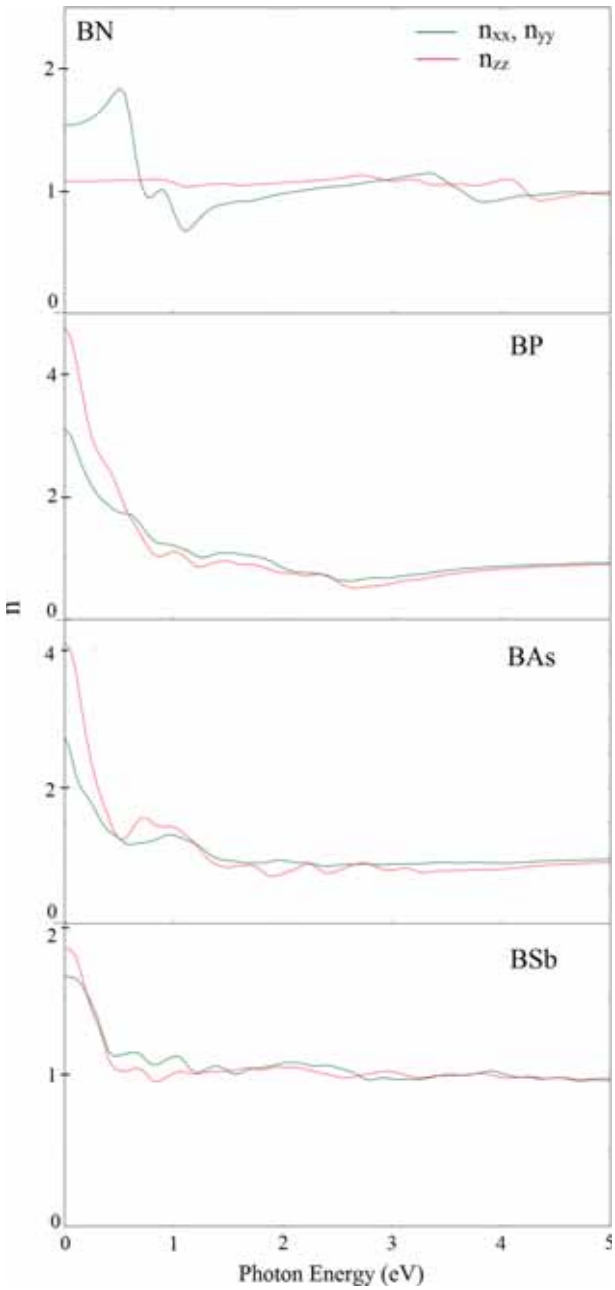

Figure 12. Refractive index of B-group V h-NWs.

From figure 10, BP h-NW has the highest static dielectric constant ($\epsilon_{\text{real}}(\omega = 0)$) of 9.66 and 22.72 in IR region, across and along the length respectively, compared to other h-NWs studied. The lowest static dielectric constant of 2.36 (across the length) and 1.16 (along the length) are observed for BN h-NW. The measured static dielectric constant follows the trend BP>BAs> BSb>BN h-NW. Figure 11 presents the imaginary part of the dielectric constant, where the observed peaks correspond to interband transitions. All these NWs show peaks majorly in the infrared (IR) range (0–1.77 eV) of the electromagnetic (EM) spectrum. BN

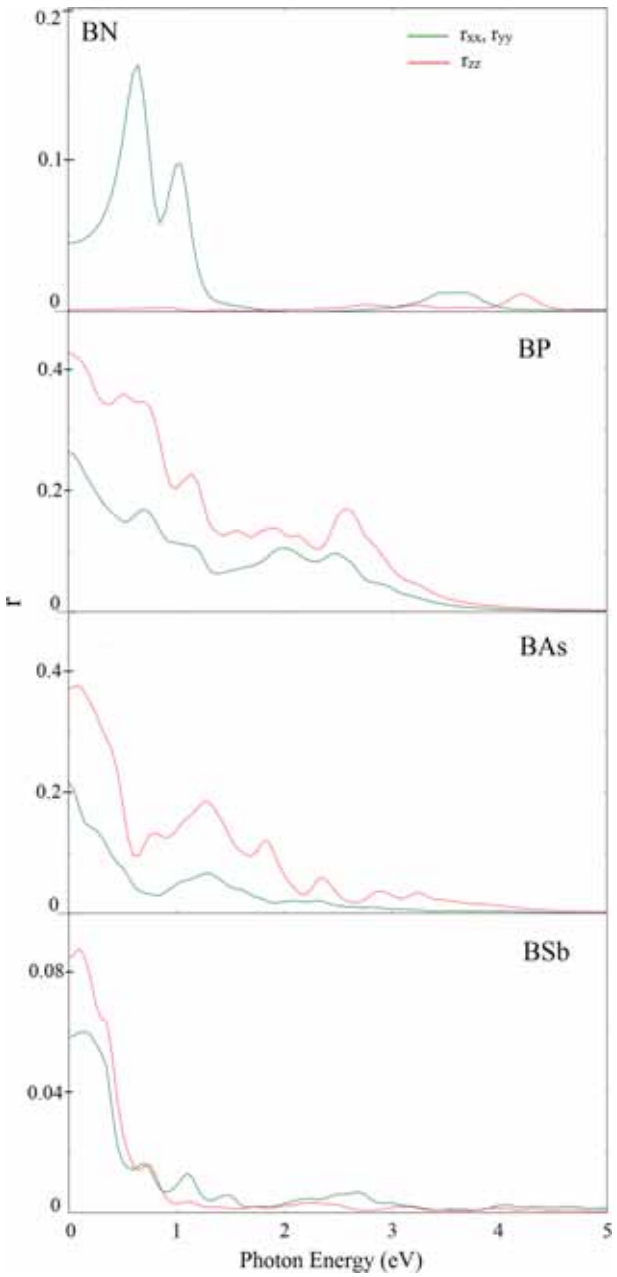

Figure 13. Reflectivity of B-group V h-NWs.

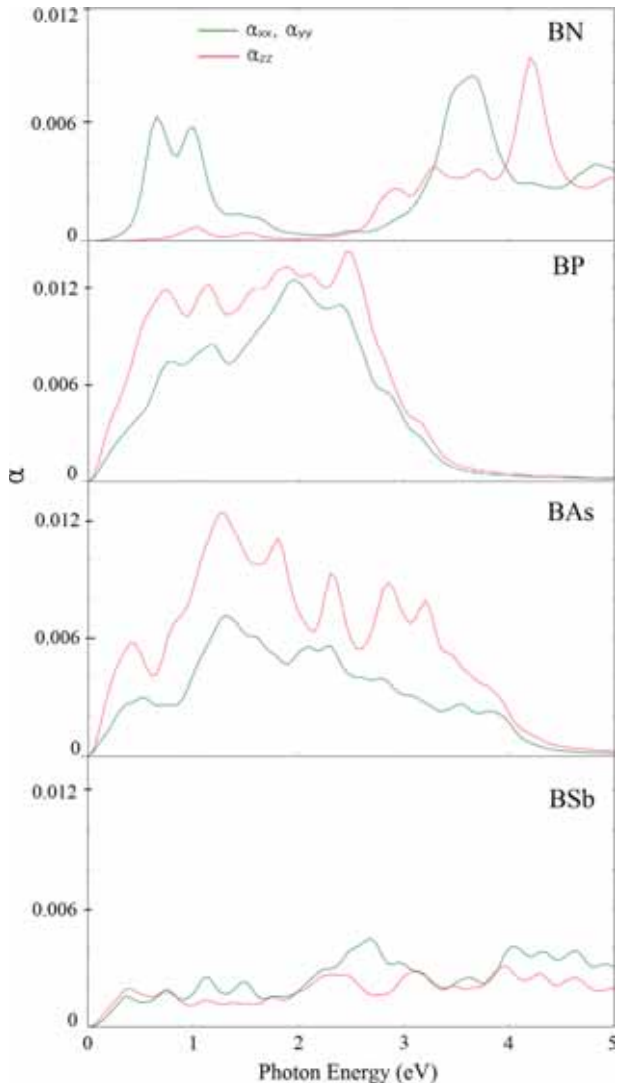

Figure 14. Absorption coefficient of B-group V h-NWs.

has $\epsilon_{real} > 0$ and $\epsilon_{imag} \approx 0$ in the visible (1.78 to 3.1 eV) and ultraviolet (UV) (3.2 to 5 eV) ranges, predicting the transparent behaviour of the NW in these regions.

Figure 12 depicts the refractive index of B-group V h-NWs as a function of photon energy. In general, refractive index offers the information about the angle of refraction the light undergoes while entering into a medium. Higher refractive index causes lesser refraction angle measured from the normal. Higher refractive indices are observed for all the four h-NWs in the IR range than in visible and UV ranges. BP h-NW has exhibited relatively highest peaks of 3.1 (across the length) and 4.76 (along the length) at 0 eV than its counterparts. The peak refractive index has followed the trend of BP > BAs > BN > BSb (across the length) and BP > BAs > BSb > BN (along the length).

The optical reflectivity of the B-group V h-NWs is plotted in figure 13, where high reflectivity is observed in the IR range, while the reflectivity observed in the UV range is near negligible. Moreover, BP h-NW is observed to possess relatively high reflectivity and BSb h-NW the least in comparison to their counterparts. Approximately zero reflectivity is observed for BN h-NW in the visible and UV ranges, support its transparent behaviour.

Absorption coefficient furnishes the information of the rate at which intensity of light decreases as it passes through the material. Absorption coefficient of a material depends on both the dielectric constant of the material and wavelength of the incident light. The

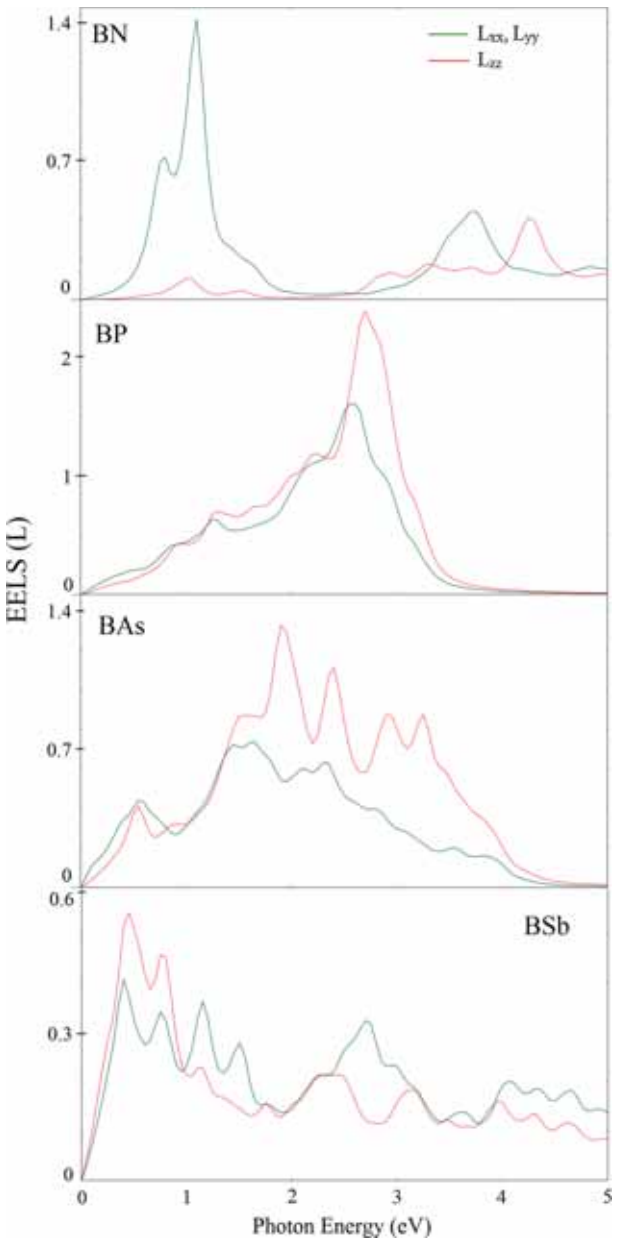

Figure 15. Electron energy loss spectra of B-group V h-NWs.

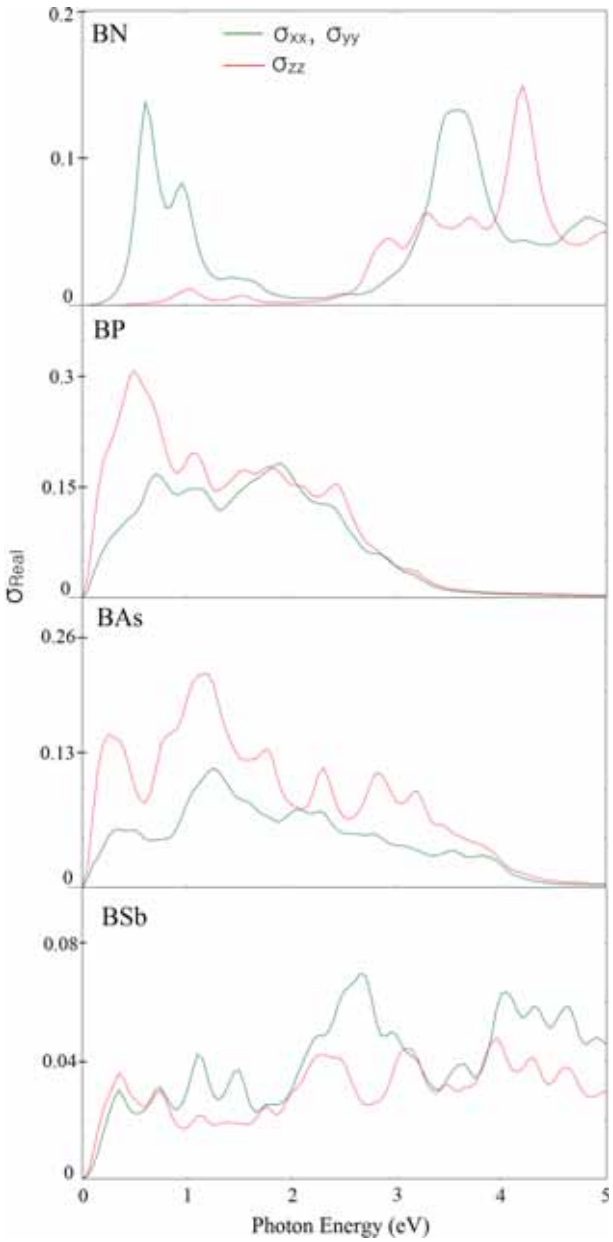

Figure 16. Real part of optical conductivity for B-group V h-NWs.

frequency-dependent absorption coefficient for the B-group V h-NWs is shown in figure 14. BP and BAs h-NWs offered good absorption at IR and visible ranges, whereas BN is observed to be more active at the UV range. Further, BP h-NW shows relatively better photon absorption than its counterparts, with peaks located at 1.9 eV (across the length) and 2.4 eV (along the length) in the visible range. BSb h-NW has a consistent but very poor absorption behaviour throughout the EM range.

The plotted EELS in figure 15 has peaks for BN h-NW at 1.1 eV (across the length) and 4.25 eV (along the length), while, for BAs h-NW at 1.6 eV (across the length) and 1.9 eV (along the length), and for BSb h-NW at 0.4 eV (across the length) and 0.44 eV (along the length). BP h-NW has the highest loss peaks at 2.6 eV (across the length) and 2.7 eV (along the length), which might be due to plasmon excitation as the corresponding dielectric function is nearly zero in that location. The remaining small peaks with non-zero dielectric function correspond to interband transitions.

The real and imaginary parts of frequency-dependent optical conductivity are plotted in figures 16 and 17, respectively. Once again, the BP h-NW dominated its counterparts with relatively high peaks at 1.9 eV (across the length) and 0.5 eV (along the length) in the real part

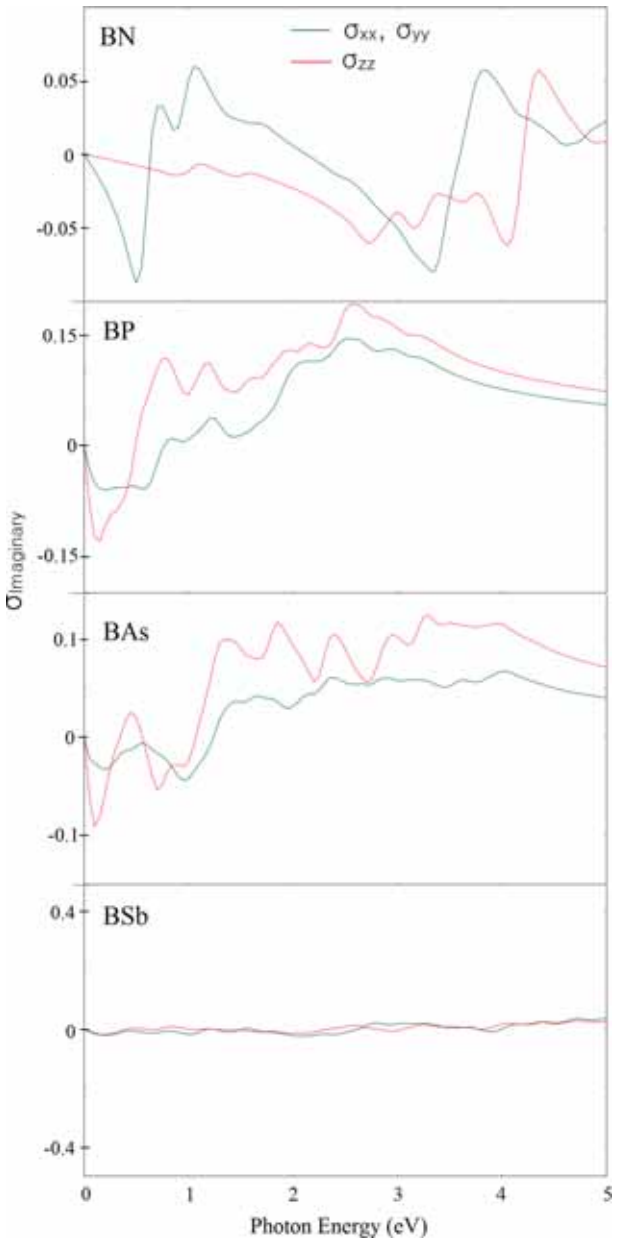

Figure 17. Imaginary part of optical conductivity for B-group V h-NWs.

of optical conductivity. This can be attributed to the high absorption coefficient of BP h-NW and deeper penetration of EM wave. The BP and BAs h-NWs exhibit high σ_{real} in the IR and visible ranges, and high $\sigma_{\text{imaginary}}$ in the visible and UV ranges. The negative values of $\sigma_{\text{imaginary}}$ observed for BN, BP and BAs h-NWs in the IR region are due to high extinction coefficient, implying reduced EM wave propagation in this region. To conclude, optical transparency of BN h-NW, and high reactivity of BP and BAs h-NWs for incident photons have been witnessed through the computed absorption coefficient, reflectivity, refractive index, optical conductivity and EELS functions.

4. Conclusion

The present paper illustrates the structural, electronic and optical properties of the B-group V h-NWs of analogous diameter of 12 Å, performed through DFT-based first principle approach. Structural analysis reveals the decreasing stability of the NWs with increasing atomic number of the group V element. The electronic nature assessed through band structure and DOS calculations reveal metallicity for BN, BP and BAs h-NWs, and semiconducting nature for BSb h-NW. The analysis of optical properties illustrates higher reactivity of BP and BAs h-NWs for light, especially in the IR and visible ranges, than their contenders. Owing to its optical transparency, metallic nature and high stability, the BN h-NW may be utilized in optoelectronic devices. Further, our theoretical observations are expected to serve as a basis for the researchers working on developing B-group V nanowire-based solar cells and optoelectronic devices.

Acknowledgements

The authors are thankful to the Board of Research in Nuclear Sciences (Department of Atomic Energy, Government of India) for the financial support under Project Grant Number 2013/37P/20/BRNS/956. The authors are also thankful to ABV-IIITM Gwalior for the infrastructural facilities provided to perform the present computational work at CNT lab.

References

[1] Katsuhiro Tomioka, Masatoshi Yoshimura and Takashi Fukui, *Nature* **488**(**7410**), 189 (2012).
[2] Jonas Johansson, Lisa S Karlsson, C Patrik, T Svensson, Thomas Martensson, Brent A Wa-caser, Knut Deppert, Lars Samuelson and Werner Seifert, *Nature Mater.* **5**(**7**), 574 (2006)
[3] F L Deepak, C P Vinod, K Mukhopadhyay, A Govindaraj and C N R Rao, *Chem. Phys. Lett.* **353**(**5**), 345 (2002)
[4] Peter Krogstrup, Henrik Ingerslev Jrgensen, Martin Heiss, Olivier Demichel, Jeppe V Holm, Martin Aagesen, Jesper Nygard and Anna Fontcuberta i Morral, *Nature Photon.* **7**(**4**), 306 (2013)
[5] Matteo Bosi and Claudio Pelosi, *Prog. Photovolt.: Res. Appl.* **15**(**1**), 51 (2007)
[6] Yajie Dong, Bozhi Tian, Thomas J Kempa and Charles M Lieber, *Nano Lett.* **9**(**5**), 2183 (2009)
[7] Jesper Wallentin *et al*, *Science* **339**(**6123**), 1057 (2013)
[8] R R LaPierre *et al*, *Phys. Status Solidi (RRL)-Rapid Res. Lett.* **7**(**10**), 815 (2013)

[9] Souichi Yoshida, Isao Tamai, Taketomo Sato and Hideki Hasegawa, *Jpn. J. Appl. Phys.* **43**(**4S**), 2064 (2004)
[10] R C Wang, Chuan-Pu Liu, Jow-Lay Huang and S-J Chen, *Appl. Phys. Lett.* **86**(**25**), 251104 (2005)
[11] Peidong Yang *et al*, *Adv. Funct. Mater.* **12**(**5**), 323 (2002)
[12] B SanthiBhushan, Sumit Kumar Jain and Anurag Srivastava, *Adv. Sci. Lett.* **21**(**9**), 2850 (2015)
[13] Atomistix ToolKit-Virtual Nanolab, Quantumwise A/S. [Online]. Available: http://quantumwise.com/, accessed Sep.12, 2015
[14] John P Perdew, Kieron Burke and Matthias Ernzerhof, *Phys. Rev. Lett.* **77(18)**, 3865 (1996)
[15] Fabien Tran and Peter Blaha, *Phys. Rev. Lett.* **102**(**22**), 226401 (2009)
[16] Optical Spectrum in ATK-VNL. [Online]. Available: https://www.quantumwise.com/documents/manuals/latest/ReferenceManual/index.html/ref.opticalspectrum.html, accessed Sep.12, 2015
[17] Ritwika Das, Suman Chowdhury, Arnab Majumdar and Debnarayan Jana, *RSC Adv.* **5**(**1**), 41 (2015)